



**HAL**  
open science

## Integrated reluctance position sensor for the self-commutation of a hybrid linear electric actuator

Pierre-Emmanuel Cavarec, Hamid Ben Ahmed, Bernard Multon

► **To cite this version:**

Pierre-Emmanuel Cavarec, Hamid Ben Ahmed, Bernard Multon. Integrated reluctance position sensor for the self-commutation of a hybrid linear electric actuator. *European Power Electronic* 2001, Aug 2001, GRAZ, Austria. 7p. hal-00674237

**HAL Id: hal-00674237**

**<https://hal.science/hal-00674237>**

Submitted on 26 Feb 2012

**HAL** is a multi-disciplinary open access archive for the deposit and dissemination of scientific research documents, whether they are published or not. The documents may come from teaching and research institutions in France or abroad, or from public or private research centers.

L'archive ouverte pluridisciplinaire **HAL**, est destinée au dépôt et à la diffusion de documents scientifiques de niveau recherche, publiés ou non, émanant des établissements d'enseignement et de recherche français ou étrangers, des laboratoires publics ou privés.

## Integrated reluctance position sensor for the self-commutation of a hybrid linear electric actuator

Cavarec Pierre-Emmanuel, Hamid Ben Ahmed, Bernard Multon  
LESIR Brittany branch  
Campus de Ker Lann 35170 Bruz  
France  
[Cavarec@bretagne.ens-cachan.fr](mailto:Cavarec@bretagne.ens-cachan.fr)

### Keywords:

Actuators, Highly dynamic drives, Linear drives, Modeling, Sensor

### Abstract

This paper presents a new design for a fully-integrated linear reluctance position sensor. Such a sensor is particularly well-adapted to compact hybrid synchronous linear actuators. A prototype has been developed and tested and a high-frequency simulation has confirmed the frequency behavior. Different types of demodulation are compared herein. A synchronous differential demodulation has been derived and yields very good results.

## 1. INTRODUCTION

Linear electromagnetic actuators are appreciated for their dynamic skills. Nevertheless they frequently suffer from a low force volume ratio. Yet, applications which require strength and speed are numerous (machine tool, active shock absorber)



*Fig. 1: The multi-airgap linear actuator prototype*

To overcome this need, an hybrid multi-airgap linear electric actuator has been realized. Several magnetic composite rod with very small steps make up the mobile part (in order to increase the effort density). This linear actuator is an hybrid synchronous one. It needs a self commutation electronics power for its three phases. This must allow to reach a maximal electrical pulsation around 200Hz which corresponds to a linear speed of 1m/s.

To realize this self commutation, it needs an accurate position sensor. This sensor must withstand the same harsh environment as the actuator itself not to decrease its performances.

Optical position sensors are ruled out owing to the price and to the harsh environment (mainly the high temperature). Linear output Hall-effect sensors technology suffer from a poor accuracy for precise adjustment of electrical angle. Linear Variable Differential Transformers (LVDT) technology gives good precision in harsh environment. Unfortunately, their limited stroke in relation to their fixed part size forbids to integrate them in our motor structure. It has actually a stator size smaller than its strokes.

A sensor with LVDT robustness and precision but with smaller length was needed. Moreover an highly integrated sensor was searched. In sum, we searched and carried out a position sensor with low size and homogeneous technology

## 2. SENSOR PRINCIPLE

This sensor is based on variable a reluctance principle. It is a magnetic circuit made up by a fixed part and a mobile one, here one of the rods of the actuator. This sensor is conceive to make the position of the rod change the circuit reluctance.

We have chosen to place two independent coils around this circuit. The first one, called the excitation coil, is supplied by an high frequency alternative current. It generates an alternative magnetic field in the magnetic circuit. The flux density in this circuit depends on the rod position. The second coil, called the measure coil, measures the flux variation. A suitable signal processing of the measure coil voltage gives a circuit reluctance image, linked to the rod position

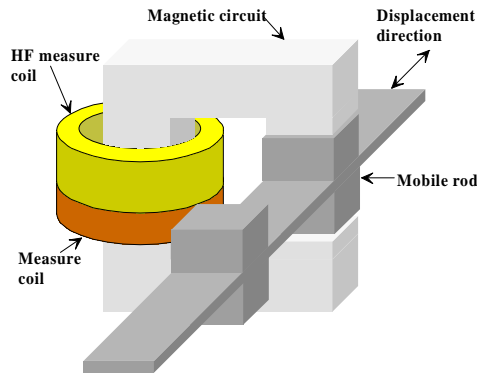


Fig 2: Linear reluctance position sensor principle

The output signal is a sinusoidal EMF modulated by the instantaneous value of the inductance. As the value of this inductance depends on the rod position, a adapted data processing can give an image of the rod position

Figure 3 below provides an example of: position, current input, output signal and demodulated signal.

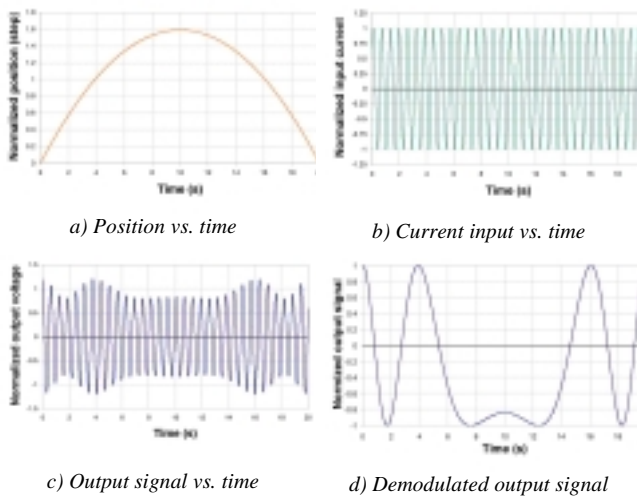
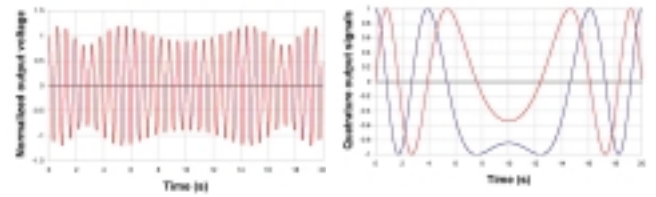


Fig. 3: Sensor input and output signals

In classical LVDT sensors, the output is the absolute position. For our application (the control of a synchronous linear actuator), a relative position

sensor is more useful than an absolute position sensor; hence, at least two sensors are necessary.



a) Second output signal vs. time    b) Two demodulated output signals  
 Fig. 4: Second output signal

As the number of harmonics decreases in the reluctance waveform, the sinus/cosinus demodulation becomes easier.

### 3. THE LINEAR POSITION SENSOR PROTOTYPE

For our linear actuator, the mobile part is composed of small-diameter cylindrical rods in massive soft magnetic iron. The rods are made up of magnetic and amagnetic disc alternations. These alternations force the longitudinal flux to circulate through the actuator. The actuator rods are thus sought to act as the mobile part of the sensor. The fixed part is made up of a magnetic ring filled by both the excitation and the measurement coil.

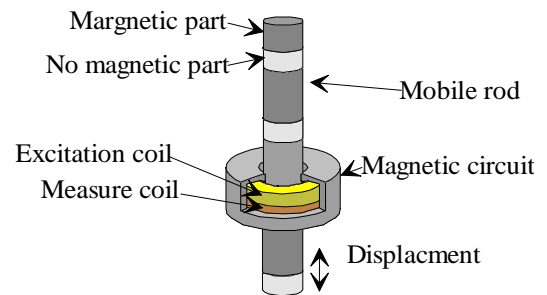


Figure 5 a): Real sensor principle



Fig 5 b): magnetic ring prototypes

In order to detect the relative position, a minimum of two transformers is needed. To obtain one signal per

phase, we have elected to use three transformers, hence three rings.

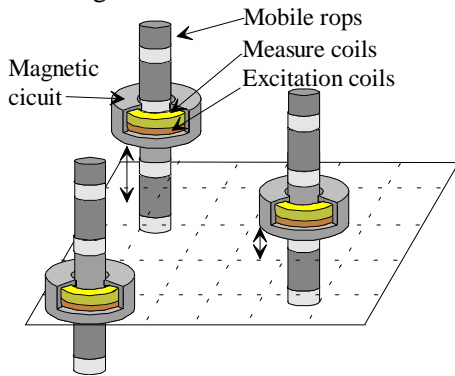


Fig. 6: Relative positions of the three sensors

All of the actuator rods are mechanically synchronous. For bulk reasons, each ring is placed around a different rod. The gap between transformer positions must be equal to one-third of the actuator step, which creates the electrical phase difference between the three output signals.

#### 4. LOW-FREQUENCY

##### TRANSFORMER MODELISATION

We have sought to present an electrical model of the sensor.

In this initial approach, the element values are independent of frequency. This condition means that the skin depth (for eddy currents) is greater than the magnetic circuit thickness. We are strictly focusing on the evolution of magnetization inductance as a function of position.

An F.E. simulation has been run in order to optimize the Ld-Lq ratio as in a variable reluctance actuator.

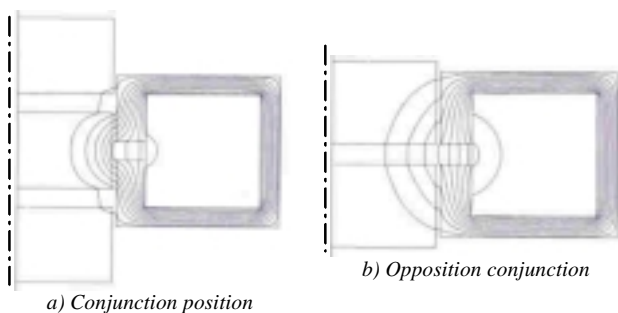


Fig. 7: Low-frequency field map  $\mu_r = 120$

This optimization procedure has provided the following inductance variation versus position profile.

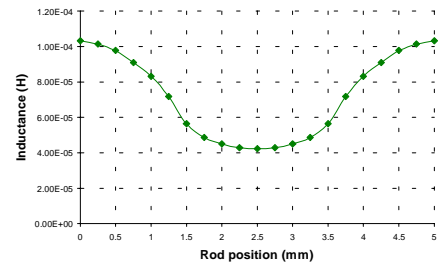


Fig. 8a: Reluctance vs. position

The harmonic decomposition of this variation is calculated in Fig. 8b below.

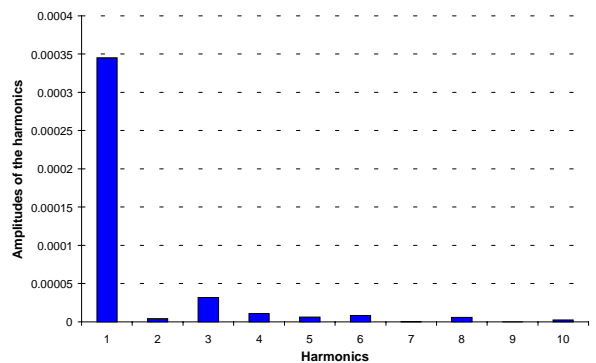


Fig. 8b: Harmonic decomposition of the variation in inductance vs. position

It can be observed that the variation in inductance displays few harmonics. According to our initial approach, we consider this variation as a pure sinus variation; hence, the relation between position and output signals will be simpler.

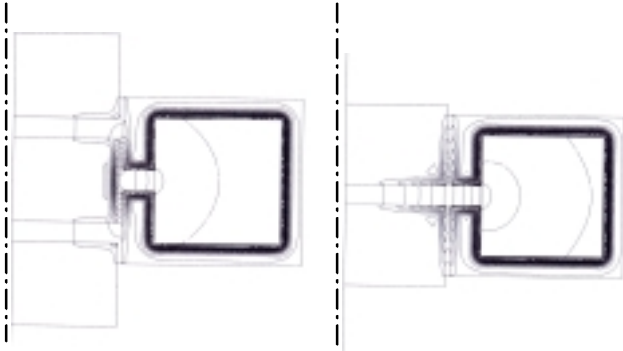
Experimental measurements show that the optimal sensitivity frequency lies around 2 kHz. In this case, the skin depth is less than the magnetic circuit thickness. Transformer model element values therefore change with frequency.

#### 5. HIGH-FREQUENCY

##### TRANSFORMER MODELISATION

A frequency study has been conducted to simulate sensor behavior and an appropriate model has been developed.

We have applied the FEM with eddy currents. Figure 10 shows magnetic field in the two extrem positions.



a) Conjunction position b) Opposition conjunction  
Fig. 9: High-frequency (1.5 kHz) field map  $\mu_r = 120, \rho = 1.4 \cdot 10^{-7} \Omega.m$

Copper losses in the magnetic circuit create a phase between the input current and the flux. Hence, we can divide the flux into both a  $0^\circ$  flux component and a  $90^\circ$  flux component (see Figure 10).

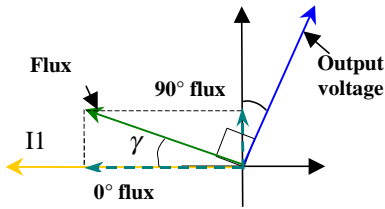


Fig. 10: Flux vector diagram

If:

$$i(t) = I_m \cdot \cos(\omega t) \quad (1)$$

and:

$$\varphi(t) = \Psi_m(\omega) \cdot \cos(\omega t - \gamma) \quad (2)$$

We then obtain:

$$\varphi(t) = \Psi_0(\omega) \cdot \cos(\omega t) + \Psi_{90}(\omega) \cdot \sin(\omega t) \quad (3)$$

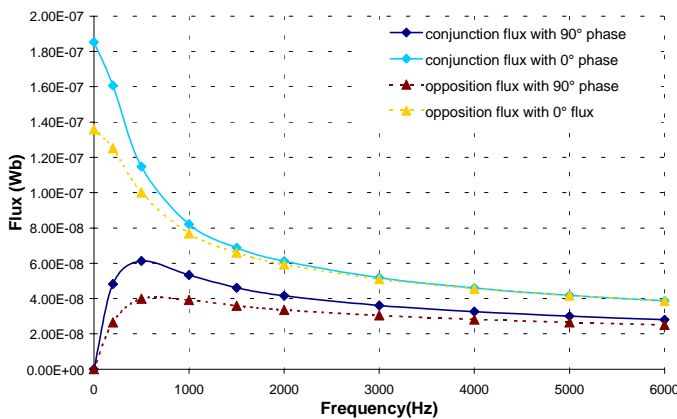


Fig. 11: Sensor flux vs. frequency

The output voltage is:

$$V_{2_{\max}} = n_2 \cdot \omega \cdot \sqrt{(\varphi_0^2 + \varphi_{90}^2)} \quad (4)$$

with:

$\omega$  the pulsation,

$i$  the current,

$\varphi_0$  the flux in phase with the current,

$\varphi_{90}$  the quadratic flux, and

$n$  the primary and secondary.

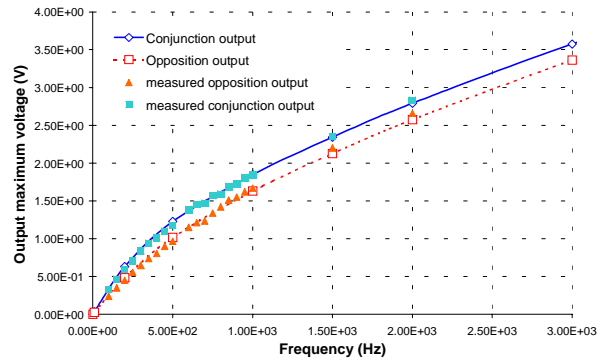


Fig. 12: Output voltage in conjunction and in opposition

It is apparent that the measurements are in close agreement with simulation values.

The output phase between the current and the flux is:

$$\theta = \arctan\left(\frac{\varphi_{90}}{\varphi_0}\right) \quad (5)$$

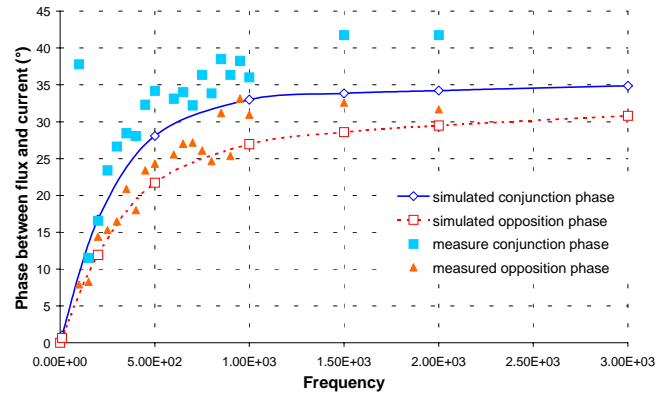


Fig. 13: Phase between the current and the flux

From this figure, the phase is more sensitive to measurement noise. However, the simulation curves do not differ significantly from measurement results. It is important to note that simulations are extremely sensitive to material characteristics. A slight mistake in these values can explain the difference between simulation and measurement results.

Since all variables are of the sinus waveform, the reactive power (i.e. the magnetic energy) is directly:

$$P_r = \frac{1}{2} \cdot \omega \cdot \varphi_0 \cdot i \cdot n_1 \quad (6)$$

The active power (i.e. the Joule losses) is:

$$P_a = \frac{1}{2} \cdot \omega \cdot \varphi_{90} \cdot i \cdot n_1 \quad (7)$$

This set-up implies that it is possible to determine the electrical scheme.

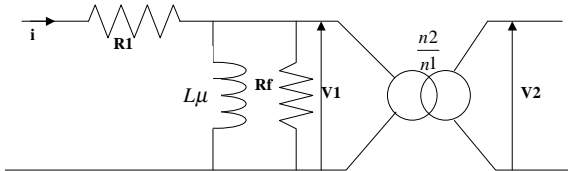


Fig. 14: The transformer model

$$P_r = \frac{1}{2} \cdot \frac{V_{2\max}^2}{L_\mu \cdot \omega} \quad (8)$$

$$L_\mu = \frac{n_2^2 \cdot (\varphi_0^2 + \varphi_{90}^2)}{\varphi_0 \cdot n_1 \cdot i} \quad (9)$$

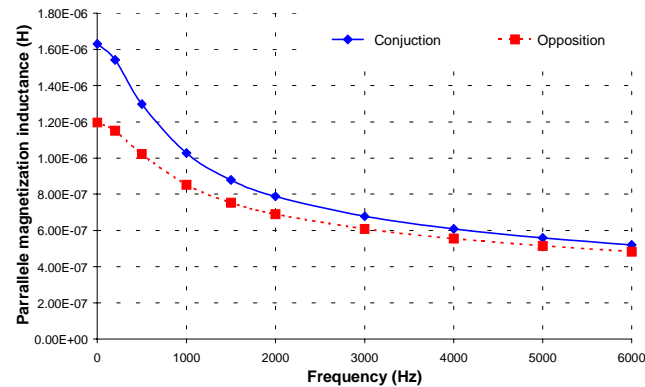
and:

$$P_r = \frac{1}{2} \cdot \frac{V_{2\max}^2}{R_\mu} \quad (10)$$

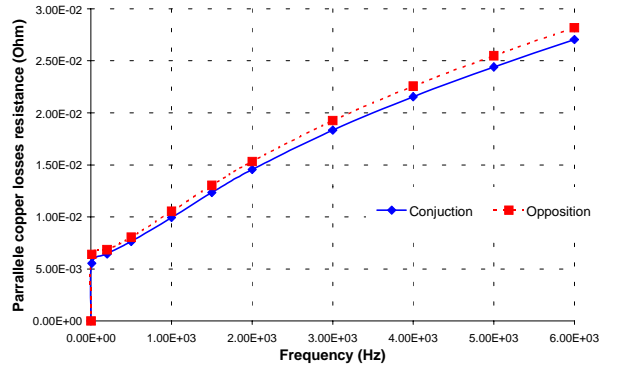
$$R_\mu = \frac{n_1 \cdot \omega \cdot (\varphi_0^2 + \varphi_{90}^2)}{\varphi_{90} \cdot i} \quad (11)$$

$$R_\mu = \frac{n_1 \cdot \omega \cdot (\varphi_0^2 + \varphi_{90}^2)}{\varphi_{90} \cdot i} \quad (11)$$

We can now calculate the variation in magnetization inductance and copper loss resistance versus frequency (see Figs. 15 a and b).



a) Magnetization inductance



b) Copper loss resistance

Fig. 15: Classical model variable vs. frequency

Both magnetization inductance and copper loss resistance depend on the frequency and the position.

## 6. DEMODULATION PRINCIPLES

The output signal should be interpreted as an AM signal. Two kinds of demodulation are possible:

- amplitude demodulation, in which we compare the maximum signal value (see Figure 16), and
- synchronous demodulation, in which we must choose a shift angle (see Figure 17).

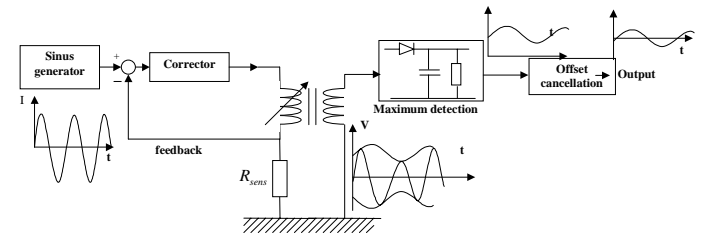


Fig. 16: The amplitude demodulation principle

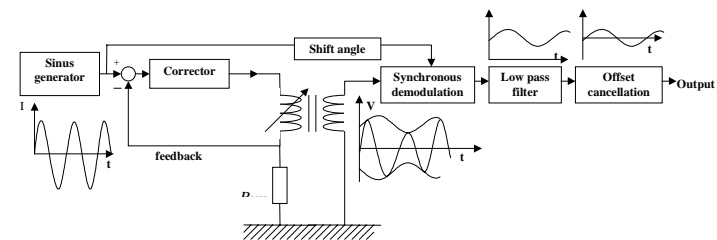


Fig. 17: The synchronous demodulation principle

For synchronous demodulation, the choice of shift angle must yield maximal sensor sensitivity, which means maximal output magnitude between two extreme positions (a half-step displacement of the rod) (see Figure 18).

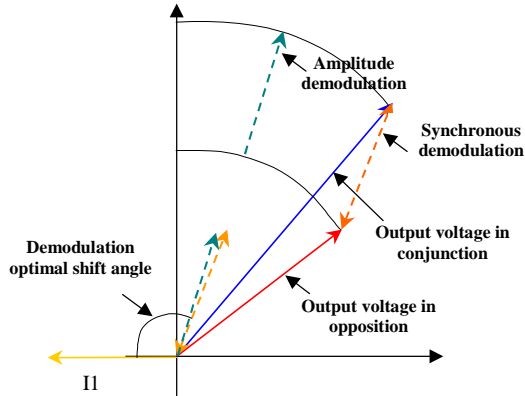


Fig. 18: Vector diagram

Synchronous demodulation combines the amplitude variation and the angle variation between the two extreme positions.

With the high-frequency simulation, we are able to compare the results of the two demodulation principles (see Figure 19).

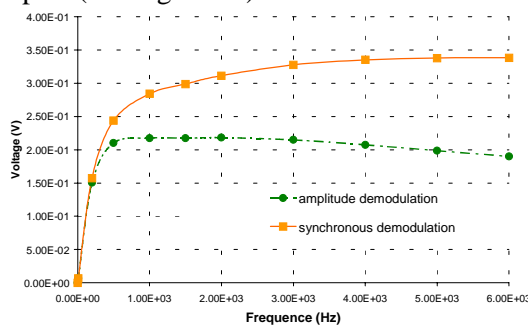


Fig. 19: Output voltage vs. frequency

Hence, synchronous demodulation always yields better results, yet with the disadvantage of a more complex demodulation circuit; we have chosen this last type.

### 7. DIFFERENTIAL MEASUREMENTS

Differential measurements entail using the difference between two coil voltage measurements: this is known as the "LVDT" method (see Figure 20).

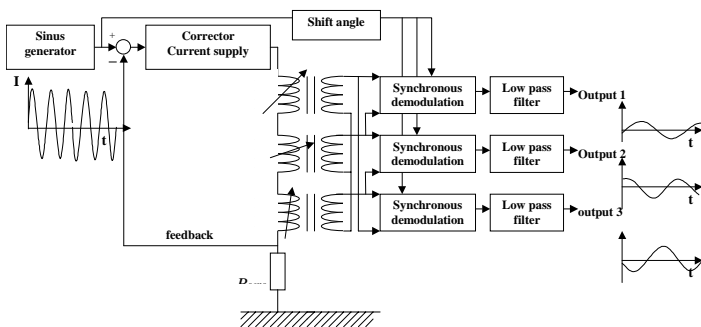


Fig. 20: Differential measurement principle

It immediately cancels the offset output signal value, without any adjustment. Moreover, it protects against temperature sensitivity.

Practically speaking, differential measurement requires low-dispersion sensor characteristics, which implies careful magnetic ring and coil configurations. With three different rings, the differential measurement makes the sum in a star-connected circuit and eliminates the offset cancellation.

### 8. MODULATION FREQUENCY CHOICE

The choice of modulation frequency depends on three parameters:

- the sensitivity of the sensor,
- the modulation current limitation, and
- demodulation complexity.

The first parameter has already been demonstrated.

The second parameter is present due to the fact that the supply voltage is limited. Magnetization inductance limits the current as frequency increases.

Lastly, as the modulation frequency increases, the demodulation low-pass filter becomes simpler and the pass-band of the sensor wider.

### 9. EXPERIMENTAL RESULTS

The sensor position has been tested. A supply and demodulation printed circuit has been created and gives good results (see Figure 21).

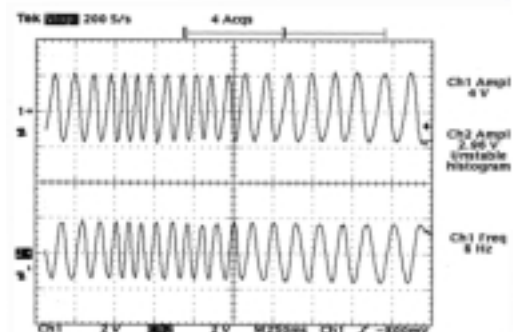


Fig. 21: Measurement of two output signals with variable rod speed

The demodulated signals are similar to a sinus/cosinus output. This finding is mainly due to the low harmonic composition of the inductance vs. position variation.

A new demodulation approach is currently being developed. To enhance the accuracy of the sensor, we have considered the output signal as a no-sinus signal. Hence, this new approach will be self-adapted to the shape of the output signal.

## 10. OTHER POSSIBLE SENSOR STRUCTURES

The three-ring structure is the simplest for this kind of sensor. It is obviously not the only possibility. Others may also display interesting proprieties. One solution is shown in Figure 22; its main advantage is the presence of a common excitation coil.

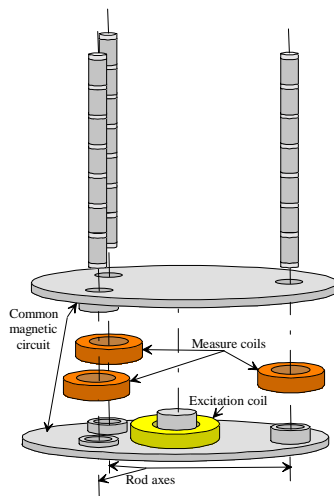


Fig. 22: Close-up view of the common excitation coil structure

The aim of this new structure is to decrease the coil dispersion sensitivity. It uses three-dimensional magnetic circuits, which in order to ensure their efficiency have to be made from iron powder.

## 11. CONCLUSION

An integrated position sensor has been developed and tested. A theoretical study of the frequency behavior has been conducted.

The advantages of both synchronous and differential demodulation have been shown and then confirmed by experimental results.

This kind of sensors is very appreciated in unconventional hybrid electric actuator applications : its structures can be adapted to all kind of mobile parts

## 12. REFERENCES

[1] B. Lequesne, and T. Schroeder , “*High Accuracy Magnetic Position Encoder Concept*”, IEEE Trans. on Ind. Appl., vol. 35, N° 3, May/June 1999, pp.568-576

[2] E Santander , “*Etude et modelisation de capteurs inductifs industriels pour la mesure de déplacement a travers la paroi d’une enceinte metallique étanche*” 1990

[3] B. Multon; M. Geoffroy, P.F. Desesquelles , “*Variable reluctance rotating shaft sensor for D.C. brushless vernier reluctance motor*”, First Japanese-French Congress of MECATRONICS, October 1992,

[4] M. Antunes-Menoita, *Modelling, conception and realisation of an high stress density multi – airgap linear actuator.* (in french) Report Engineer CNAM-ENS de Cachan, nov. 1999.

[5] A. Amouri, C Rioux, J. Lucidarme, P.F. Desesquelles et H. Ben Ahmed, “*Modelling and experiments of a longitudinal multi-airgap linear Reluctance Actuator.*”, Imacs Symposium MCTs Lille 1991, vol1, pp 214 220